Valley-Hall kink and edge states in multilayer graphene

Jeil Jung, Fan Zhang, Zhenhua Qiao, and Allan H. MacDonald
Department of Physics, University of Texas at Austin, USA
(Received 18 May 2011; published 5 August 2011)

We report on a theoretical study of one-dimensional (1D) states localized at few-layer graphene system ribbon edges and at interfaces between few-layer graphene systems with different valley-Hall conductivities. These 1D states are topologically protected when valley mixing is neglected. We address the influence on their properties of stacking arrangement, interface structure, and external electric field perpendicular to the layers. We find that 1D states are generally absent at multilayer ribbon armchair direction edges, but present irrespective of crystallographic orientation at any internal valley-Hall interface of an ABC-stacked multilayer.

DOI: 10.1103/PhysRevB.84.075418 PACS number(s): 73.22.Pr, 03.65.Vf, 73.43.−f, 81.05.ue

I. INTRODUCTION

Metallic surface states in a system with an insulating bulk are often related to topological order.[1] An important example is provided by the quantum Hall effect of two-dimensional (2D) systems in the presence of an external magnetic field, in which two-dimensional (1D) edge states[2] accompany integer-valued Chern indices[3] of bulk 2D bands. The recent identification of topological-insulator materials[4] has provided a new example, one which does not rely on external magnetic fields. In topological insulators, strong spin-orbit interactions yield bulk bands that have nontrivial values of a Z_2 topological index and support topologically protected surface states. The present study explores a 2D bulk example in which the relevant topological index is, as in the quantum Hall case, an integer-valued Chern index even though no magnetic field is present.

Our work is motivated by the suggestion of Martin, Blanter, and Morpurgo[5] that 1D states can be induced in bilayer graphene by changing the sign of an interlayer electric field. (Below, electric field will always refer to a field directed between the layers of a few-layer graphene system.) These states have a formal structure similar to that of the zero modes that appear in the A phase of ^{3}He thin films at domain walls between regions with opposite spontaneous orbital moments.[6] They have been studied as a special kind of tunable Luttinger liquids[7] and are expected to influence 2D transport in the presence of periodic potential modulations in superlattices.[8] The 1D states in Ref. 5 can be understood as being a consequence of separate Chern indices of opposite sign associated with the K and K' Dirac points of bilayer graphene. The property that these Chern numbers are implied by the momentum-space Berry curvature of bilayer-graphene bands[9] when the electric field is nonzero is referred to as the valley-Hall effect. The valley Chern numbers emerge when the electric field breaks inversion symmetry to open a gap in the 2D bulk bilayer electronic structure. However, because the two valleys share the Brillouin zone of a bilayer graphene crystal, separate Chern numbers are never precisely defined and are, strictly speaking, an artifact of the commonly employed continuum $\vec{k}\cdot\vec{p}$ electronic structure model. Correspondingly, the 1D states that are the subject of Ref. 5 are not guaranteed to be present at all energies and are not topologically protected against perturbations that couple different valleys. The goal of the present study is to assess the degree to which these caveats are practically important.

1D states of the type we consider were first found in numerical studies of zigzag bilayer ribbons,[10] and later recognized as valley-Hall edge states by Morpurgo *et al.*[13] They have also been previously studied theoretically in single-layer graphene samples with an imposed staggered potential,[14,15] i.e., a potential that has opposite signs on the graphene honeycomb A and B sublattices. A more detailed analysis of the correspondence between bulk and edge in bilayer graphene has been carried out recently, concluding that the existence of 1D states at an edge depends on its morphology.[16] In the present paper, we consider both bilayer graphene and other few-layer graphene systems in which electric fields open up an energy gap and yield a valley-Hall effect. Continuum model considerations suggest that 1D states should be present at the edge of graphene ribbons with a valley-Hall effect and at interfaces between systems with different valley-Hall-effect quantum numbers. We will refer to the former type of 1D state as an edge state and to the latter as a kink state. In the case of bilayer graphene, for example, an interface that supports kink states is easily produced by changing the sign of the electric field along a line inside the material. To create the corresponding 1D kink states in monolayer graphene, it would be necessary to change the sign of the staggered potential.

In this paper, we use π-band tight-binding models to assess the influence of stacking orders and edge geometries on edge- and kink-state properties. As in the bilayer case, we find that the valley-Hall edge states in multilayers do not survive for armchair edge terminations. However, kink states are clearly present for both zigzag and armchair crystallographic orientations of an internal interface along which the valley-Hall quantum number changes. Section II contains the main results of our work. We start discussing the valley-Hall conductivity in terms of the low-energy continuum model of ABC-stacked N-layer graphene. We conclude that we can normally expect N 1D kink-state branches per valley localized along electric field sign-change lines. Then we use π-orbital tight-binding calculations on multilayer ribbons to test the continuum model, presenting results for the energy bands of valley-Hall edge and kink states for a number of different cases. Finally, in Sec. III, we close with a brief summary and a discussion of our findings.

II. VALLEY-HALL EDGE AND KINK STATES IN MULTILAYER GRAPHENE

The electronic-structure results for the multilayer-graphene ribbons presented here were obtained using a π-orbital tight-binding model Hamiltonian with nearest-neighbor hopping and a lattice-position-dependent external potential U_i:

$$H = -\sum_{\langle i,j \rangle} \gamma_{i,j}\ c_i^\dagger c_j + \sum_i U_i\ c_i^\dagger c_i. \qquad (1)$$

The hopping amplitude $\gamma_{i,j}$ we used is equal to $t = 2.6$ eV for in-plane hopping and $t_\perp = 0.34$ eV for out-of-plane hopping. Operators $c_i^\dagger$ and c_j are creation and destruction operators at ith and jth lattice sites. This model can yield 1D edge state or kink-state branches at energies inside bulk gaps, which can be explained qualitatively in terms of the model's bulk valley-Hall effect. This quantum valley-Hall effect and its edge states are robust to long-range disorder potentials, magnetic or not, as long as the system is free of valley scattering perturbations.[17] We start by discussing the valley-Hall properties of multilayer systems using a low-energy model Hamiltonian before returning to tight-binding model calculations carried out for ABA- and ABC-stacked bilayer, trilayer, and tetralayer graphene ribbons. We consider a variety of different examples that capture some essential features of stacked multilayer electronic structure.

A. Valley-Hall effect and associated 1D states in chirally stacked N-layer systems

The low-energy Hamiltonian in ABC-stacked (rhombohedral) N-layer graphene is useful as a simplified route for gaining insight of the system despite the simplifying assumptions. In particular, the valley-Hall properties of ABC-stacked (rhombohedral) N-layer graphene can be derived from a low-energy band structure in which Bloch states are localized mainly on top and bottom layers. Because the phase difference between top- and bottom-layer wave-function components varies more rapidly with momentum direction (measured from the K and K' Dirac points) in larger N systems, the valley Chern numbers increase with N.[18,20] To be more precise, the wave functions of the states closest to the Fermi level reside mostly on the top- and bottom-layer lattice sites without a vertical neighbor, and the valley Chern number in the presence of an electric field is equal to $N/2$ except, possibly, at very low carrier densities and weak electric fields where weak band-structure features can play a role. (Note that for odd N, this quantity is not an integer; we nevertheless refer to the values as Chern indices for convenience.) The sites with vertical neighbors have more weight in higher energy bands.

Strictly speaking, Chern numbers should be calculated by integrating Berry curvatures over the whole Brillouin zone, including contributions from near both K and K' points. This total Chern number always vanishes, as it must, when time-reversal symmetry is not violated. In the continuum model approximation, however, we can speak of valley-resolved contributions to Chern numbers because the valley indices are clearly distinguished. In this picture, familiar quantum Hall considerations suggest the presence of 1D channels at edges and along lines where the valley-Hall conductivity changes. The microscopic tight-binding model calculations we perform are intended to test the degree to which these considerations are reliable.

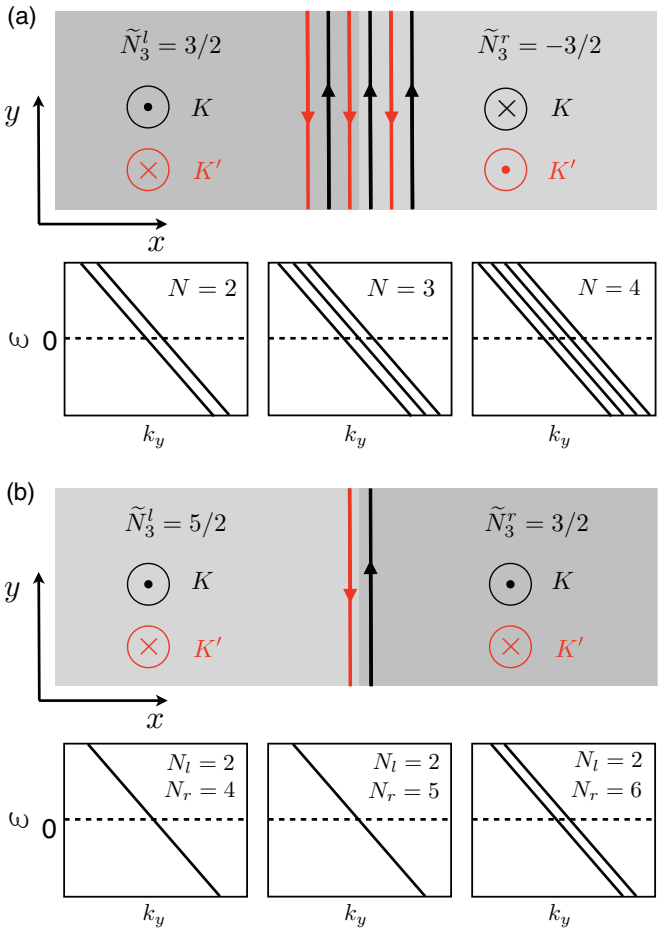

FIG. 1. (Color online) Schematic illustration of the relationship between valley-Hall effects and 1D conduction channels at interfaces expected on the basis of continuum model considerations. The number of 1D modes per valley is an integer n evaluated from differences between valley Chern numbers $n = |\widetilde{N}_3^l - \widetilde{N}_3^r|$. When the layer number N is odd, the integral of the Berry curvatures is half-odd integer, a property that is related to the half-quantized Hall effect of Dirac systems. We find that the number of 1D channels is then usually reduced to the integer part of the integrated Berry-curvature difference. The sense of the arrows directed perpendicular to the page indicates the sign of the Chern number associated with each valley. *Upper panel*: illustration of ABC trilayer graphene with opposite electric-field signs in the left and right regions with three 1D modes per valley. *Lower panel*: junction formed between pentalayer and trilayer regions under a uniform bias potential. In this case, the valley-Hall conductivities have the same sign but different magnitude on the opposite sides of the interface and the number of 1D channels is expected to be proportional to the difference of the individual Berry-curvature integrals. The continuum model picture illustrated here can be invalidated by atomic-scale physics at the interface, particularly when the number of layers on opposite sides of the interface is different.

Our working assumption in this section is that the following effective continuum model[18,21] captures essential properties of the full Hamiltonian:

$$H_N = -t_\perp \begin{pmatrix} 0 & v^{\dagger N} \\ v^N & 0 \end{pmatrix} + \frac{1}{2}\begin{pmatrix} \Delta & 0 \\ 0 & -\Delta \end{pmatrix}, \qquad (2)$$

where $-t_\perp$ is the interlayer hopping parameter, $v = v_F\pi/t_\perp$, $v_F \sim c/300$ is the Fermi velocity of single-layer graphene, $\pi = \hbar(\tau_z k_x + i k_y)$, where $\tau_z = \pm 1$ labels the K and K' valleys, (k_x,k_y) is crystal momentum measured from a Dirac point, and Δ is the potential difference between layers produced by the electric field. This Hamiltonian leads to momentum-space Berry curvatures that are sharply peaked near $(k_x,k_y) = 0$. The valley Chern numbers are obtained[5,6,9,21] by integrating the Berry curvature over 2D momenta (k_x,k_y) continued to ∞ to obtain $C_{\tau_z} = N\tau_z \mathrm{sgn}(\Delta)/2$. The valley Chern numbers are sometimes referred to as topological charges and they are denoted by $\widetilde{N}_3$ as a reminder that the topology indices of gapped 2D systems may be thought of as a dimensional reduction of topological charge N_3 at gapless 3D Fermi points.[6] The contribution to the Hall conductivity from a particular valley is $\sigma_{xy}^{\tau_z} = \widetilde{N}_3 e^2/h$. In a continuum model, the number of 1D channels per valley at an interface between two bulk regions with different valley-Hall conductivities, $\sigma_{xy}^{\tau_z} = \widetilde{N}_3\, e^2/h$, is equal to the difference between their valley Chern numbers.[5,6,15] For ballistic transport, each channel contributes e^2/h to the two-probe conductance. When the sign of the electric field is reversed at an interface, the Chern-number difference is $2 \times (N/2) = N$, which is equal to the layer number as illustrated schematically in Fig. 1.

The generalization of the notion of a valley-Hall conductivity from one- and two-layer systems to general N-layer systems can also be made using the explicit equations for the 1D interface states by following a procedure similar to that outlined in Ref. 5:

$$\begin{aligned} -V(x)u + K_N(\partial_x + k_y)^N v &= \varepsilon u, \\ K_N(\partial_x - k_y)^N u + V(x)v &= \varepsilon v. \end{aligned} \qquad (3)$$

Here, $K_N = -t_\perp(-i\, v_F\hbar/t_\perp)^N$, N is the number of layers in the system, and $V(x)$ is a general position-dependent function, which specifies the difference between top- and bottom-layer potentials. In the following sections, we will present tight-binding calculations for multilayers for a variety of different external potential profiles and discuss the validity of the qualitative picture summarized in Fig. 1.

B. Multilayer ribbons under a uniform electric field

The simplest example of valley-Hall edge states are those that appear in ABC-stacked multilayers under a uniform external electric field. The tight-binding band structure of bilayer-graphene ribbons by Castro *et al.*[10,21] has demonstrated the presence of metallic edge states, which cross the Fermi level in neutral zigzag-terminated bilayer ribbons and in chirally stacked multilayer zigzag ribbons. The edge-state properties of multilayer graphene[11] and band gaps in the presence of an electric field depend on the layer stacking.[12] The number of valley-Hall edge-state branches in each propagation direction is equal to $(N/2)$[21]. Changing either edge termination or stacking sequence introduces qualitative changes in the ribbon band structure as we now describe.

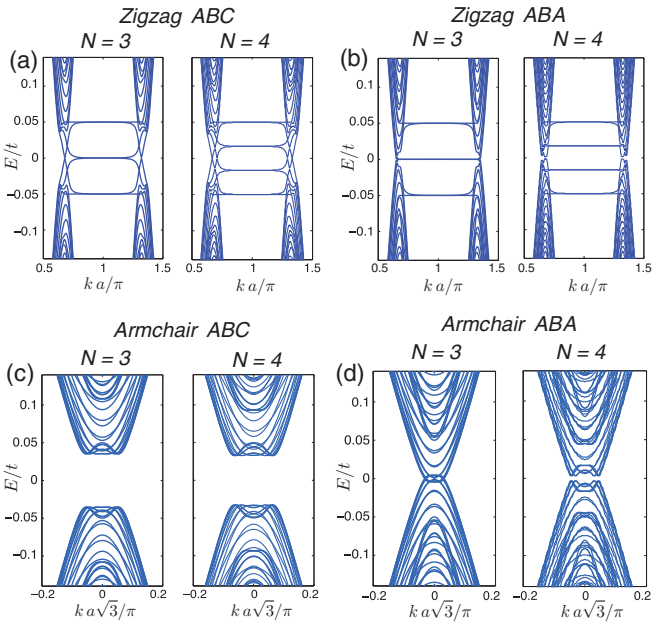

FIG. 2. (Color online) Band structures of ABC- and ABA-stacked, zigzag- and armchair-terminated trilayer and tetralayer ribbons in the presence of a uniform electric field. (a) ABC-stacked layers with zigzag edges, (b) ABA-stacked layers with zigzag edges, (c) ABC-stacked layers with armchair edges, and (d) ABA-stacked layers with armchair edges. In each figure, the left and right panels represent trilayer and tetralayer ribbons, respectively. For ABC stacking the electric field opens a bulk band gap containing edge states in the zigzag case but not in the armchair case. The number of edge-state branches is independent of the ribbon width, whereas the number of bulk-state branches is proportional to ribbon width. In the case of ABA stacking, ribbons are metallic in the trilayer, whereas a small gap opens in the tetralayer geometry.

In Fig. 2, we plot band structures for ABC- and ABA-stacked, zigzag- and armchair-terminated trilayer and tetralayer ribbons. In all these calculations, we have maintained the same interlayer potential difference $\Delta/t = 0.1$ between top and bottom layers and have taken the electric field to be uniform. In the tetralayer case, we used a smaller potential difference $\Delta' = \Delta/3$ to account for the smaller interlayer distance of the inner layers, which facilitates distinguishing their edge-state bands associated with respect to the outer ones. In multilayer zigzag ribbons with ABC stacking, the uniform electric field generates a band gap in the sample bulk[20] with edge states in the gaps. In agreement with previous analysis,[21] we find $(N/2)$ valley-Hall edge states in an N-layer ribbon in each valley that propagate in opposite directions and are localized at opposite edges. Hence, for zigzag edges the number of 1D states at the physical boundaries of the ribbons with vacuum can also be discussed in terms of valley Chern number differences between the bulk region and the vacuum $\widetilde{N}_3^{\mathrm{vac}} = 0$. In the armchair termination, both K and K' valleys appear at the same projected 1D momentum and the Hall edge states are annihilated. This observation is helpful in distinguishing edge and kink states in ribbons with internal electric-field sign changes.

For biased ABA multilayer zigzag ribbons, the system also has conducting edge states, but their pattern is more complex than in the ABC case. (Bulk and edge ribbon bands can in general be distinguished by their dependence on ribbon width.[19]) In ABA-stacked trilayer ribbons, an external bias increases the number of bulk channels while it opens a bulk gap in the ABC case.[20,22,23]

C. ABC-stacked zigzag and armchair multilayer ribbons with kink states

We have just seen that a biased bilayer and ABC trilayer graphene ribbons are gapped in the bulk but have metallic valley-Hall edge states crossing the Fermi level when they have a zigzag edge termination. Now we consider ribbons with an electric-field sign change at the ribbon center that is expected to produce N 1D channels in each valley. In these ribbons, the regions near the ribbon border will show valley-Hall edge states similar to those present in a bilayer with a uniform electric field. In Fig. 3, we plot the band structures of bilayer, trilayer, and tetralayer ribbons with zigzag edge terminations subject to a step-like interlayer potential discussed earlier.

In zigzag-terminated ribbon geometries, the K and K' momentum projections appear at the two valley points located at $k = 2\pi/3a, 4\pi/3a$ and can therefore easily be distinguished.[24] In agreement with the continuum-model analysis presented in Sec. II, we see N bands of confined kink states with a well-defined propagation direction for each valley K or K' crossing the Fermi level. Each valley has doubly degenerate additional metallic edge-state branches, with a velocity opposite to that of the confined states. In the uniformly biased case, edge states in a given valley that are localized on opposite edges have opposite propagation directions, whereas they propagate in the same direction when a kink is present. For ribbons with inversion symmetry, at the ribbon center, the copropagating edge-state channels are degenerate.

As mentioned previously, the projection of the 2D bands of graphene to obtain the ribbon band structure places K and K' valleys at the same momentum in the armchair edge case. Therefore, unlike the case of the zigzag ribbons, it is not possible to identify valley labels from ribbon band-structure plots. In the case of edge states, these difference eliminates the 1D channels completely. As we see in Fig. 3, this is not the case for ribbon states, which appear to be as robust in armchair and zigzag directions. When the electric field profile has sharp spatial variation, there is a barely visible gap opening, similar to the one found in a direction of graphene under a staggering potential.[14] This gap size decreases quickly when the potential variation at the domain becomes smoother.

In the band structures of bilayer, trilayer, and tetralayer graphene armchair ribbons subject to a kink-step bias around the ribbon center, one can clearly identify two, three, and four 1D states for each propagation direction, corresponding to confined states at the domain wall for wave vectors around $k \sim 0$ where both right- and left-going states coexist with similar Bloch function wave vectors. In armchair edges, we do not find edge-localized states crossing the Fermi level as we had found for the zigzag-terminated systems.

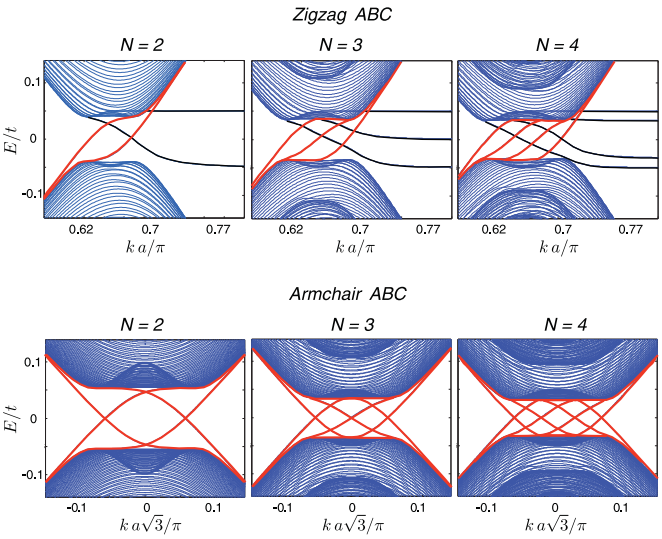

FIG. 3. (Color online) Upper Panel: band structure of bilayer, trilayer, and tetralayer graphene zigzag ribbons with an electric-field sign change at the ribbon center. We can clearly observe two, three, and four 1D valley-Hall kink states with a common sign of velocity located around the valley point. The branches, which correspond to wave functions localized at the ribbon center, are plotted in red. The other branches that cross the bulk gap are doubly-degenerate edge states. Lower Panel: band structure of bilayer, trilayer, and tetralayer graphene armchair ribbons with an electric-field sign change at the ribbon center. As in the zigzag case, we can clearly identify two, three, and four three 1D kink-state branches. In armchair edges, we do not find 1D edge-state channels.

III. SUMMARY AND CONCLUSIONS

External electric fields between layers give rise to gaps at the carrier neutrality point in bilayer and ABC multilayer graphene systems leading to quantum valley-Hall effect with $(N/2)$ chiral edge states in zigzag edge terminations. We have shown that in addition, 1D transport channels appear along lines where the sign of the inversion-symmetry-breaking potential changes. This finding generalizes results obtained previously for the bilayer[5] and monolayer cases.[14,15] The number of these metallic 1D kink state branches is proportional to the number of layers N and can be related to the bulk valley-Hall conductivity.[21] The states we have considered arise at the boundary between two regions with opposite valley-Hall conductivity. Because the Hall conductivity changes sign in opposite directions in the two valleys, both valleys produce 1D kink states and they propagate in opposite directions.

Similar valley-Hall effect considerations suggest that kink states should occur at boundaries between ribbons with different thicknesses. Our π-orbital tight-binding model calculations for ribbons with a trilayer/tetralayer boundary find that the interface electronic structure depends on whether the stacking sequence is ABC or ABA. Bulk valley-Hall effect values are also unreliable at the edge; in particular, we find that edge states are absent in multilayer armchair-terminated ribbons, as found earlier in the bilayer or monolayer case. This finding is perhaps expected since the 1D momentum projection

does not distinguish valleys in this case. It is the robustness of the kink states at internal electric-field sign changes that is perhaps the surprise. It is important to determine if it persists in the presence of disorder and turns in the propagation path.[25]

ACKNOWLEDGMENTS

The authors acknowledge helpful discussions with Qian Niu. Financial support was received from Welch Foundation grant TBF1473, NRI-SWAN, and DOE grant Division of Materials Sciences and Engineering DE-FG03-02ER45958.

[1] Y. Hatsugai, Phys. Rev. Lett. **71**, 3697 (1993).
[2] B. I. Halperin, Phys. Rev. B **25**, 2185 (1982).
[3] D. J. Thouless, M. Kohmoto, M. P. Nightingale, and M. den Nijs, Phys. Rev. Lett. **49**, 405 (1982); Q. Niu, D. J. Thouless, and Y.-S. Wu, Phys. Rev. B **31**, 3372 (1985).
[4] M. Z. Hasan and C. L. Kane, Rev. Mod. Phys. **82**, 3045 (2010).
[5] I. Martin, Ya. M. Blanter, and A. F. Morpurgo, Phys. Rev. Lett. **100**, 036804 (2008).
[6] G. E. Volovik, *The Universe in a Helium Droplet* (Oxford University Press, New York, 2003).
[7] M. Killi, T.-C. Wei, I. Affleck, and A. Paramekanti, Phys. Rev. Lett. **104**, 216406 (2010).
[8] M. Killi, S. Wu, and A. Paramekanti, e-print arXiv:1104.0051 (unpublished).
[9] D. Xiao, W. Yao, and Q. Niu, Phys. Rev. Lett. **99**, 236809 (2007).
[10] E. V. Castro, N. M. R. Peres, J. M. B. Lopes dos Santos, A. H. Castro Neto, and F. Guinea, Phys. Rev. Lett. **100**, 026802 (2008).
[11] E. V. Castro, N. M. R. Peres, and J. M. B. Lopes dos Santos, Eur. Phys. Lett. **84**, 17001 (2008).
[12] A. A. Avetisyan, B. Partoens, and F. M. Peeters, Phys. Rev. B **79**, 035421 (2009); **80**, 195401 (2009); **81**, 115432 (2010).
[13] J. Li, I. Martin, M. Büttiker, and A. F. Morpurgo, Nat. Phy. **7**, 38 (2011).
[14] G. W. Semenoff, V. Semenoff, and F. Zhou, Phys. Rev. Lett. **101**, 087204 (2008).
[15] W. Yao, S. A. Yang, and Q. Niu, Phys. Rev. Lett. **102**, 096801 (2009).
[16] J. Li, A. F. Morpurgo, M. Büttiker, and I. Martin, Phys. Rev. B **82**, 245404 (2010).
[17] Z. Qiao, Y. Yao, S. A. Yang, B. Wang, and Q. Niu, Phys. Rev. B **84**, 035431 (2011).
[18] H. Min and A. H. MacDonald, Phys. Rev. B **77**, 155416 (2008).
[19] L. Brey and H. A. Fertig, Phys. Rev. B **73**, 235411 (2006).
[20] F. Zhang, B. Sahu, H. Min, and A. H. MacDonald, Phys. Rev. B **82**, 035409 (2010).
[21] F. Zhang, J. Jung, G. A. Fiete, Q. Niu, and A. H. MacDonald, Phys. Rev. Lett. **106**, 156801 (2011).
[22] M. Koshino and E. McCann, Phys. Rev. B **80**, 165409 (2009).
[23] M. Koshino, Phys. Rev. B **81**, 125304 (2010).
[24] K. Nakada, M. Fujita, G. Dresselhaus, and M. S. Dresselhaus, Phys. Rev. B **54**, 17954 (1996).
[25] Z. Qiao, J. Jung, Q. Niu, and A. H. MacDonald, Nano Lett. **11**, 2579 (2011).